Percoco, G.; Guerra, MG.; Sánchez Salmerón, AJ.; Galantucci, LM. (2017). Experimental investigation on camera calibration for 3D photogrammetric scanning of micro-features for micrometric resolution. The International Journal of Advanced Manufacturing Technology. 91(9-12):2935-2947. https://doi.org/10.1007/s00170-016-9949-6

JrnlID 170_ArtID 9949_Proof# 1 - 03/01/2017

Int J Adv Manuf Technol
DOI 10.1007/s00170-016-9949-6

ORIGINAL ARTICLE

Experimental investigation on camera calibration for 3D photogrammetric scanning of micro-features for micrometric resolution

Q1 Gianluca Percoco [1] · Maria Grazia Guerra [1] · Antonio Jose Sanchez Salmeron [2] · Luigi Maria Galantucci [1]

Received: 5 August 2016 / Accepted: 20 December 2016

Abstract Recently, it has been demonstrated that photogrammetry can be used for the measurement of small objects with micro-features, with good results and lower cost, compared to other established techniques such as interferometry, conoscopic holography, and 3D microscopy.

Calibration is a critical step in photogrammetry and the classical pinhole camera model has been tested for magnifications lower than 2×. At higher magnification levels, because of the reduction of the depth of field (DOF), images can lead to calibration data with low reprojection errors. However, this could lead to bad results in the 3D reconstruction.

With the aim of verifying the possibility of applying the camera model to magnifications higher than 2×, experiments have been conducted using reflex cameras with 60 mm macro lens, equipped with the combination of three extension tubes, corresponding to 2.06, 2.23, and 2.4 magnification levels, respectively.

Experiments consisted of repeating calibration five times for each configuration and testing each calibration model, measuring two artifacts with different geometrical complexity. The calibration results have shown good repeatability of a subset of the internal calibration parameters. Despite the differences in the calibration reprojection error (RE), the quality of the photogrammetric 3D models retrieved was stable and satisfying.

The experiment demonstrated the possibilities of the photogrammetric system presented, equipped to very high magnification levels, to retrieve accurate 3D reconstruction of micro-features with uncertainties of few micrometers, comparable with industry's expensive state-of-the-art technologies.

Keywords Calibration · Reprojection error · 3D photogrammetric scanning Q2

1 Introduction

The constant and ever growing request for smaller components in all manufacturing fields, such as Information Technologies, Micro Electro-Mechanical systems (MEMS) for medical and biomedical applications, automotive components, is leading to a reassessment of each single task of the production process chain, from designing to controlling and measuring [1].

Together with the development of production systems, the measurement and 3D scanning systems [2], suitable for micro applications, are required to verify shape and size of micro-components.

In the 3D micro-scanning field, several technologies are still under experimentation but optical systems have important advantages if compared to other technologies.

Among optical systems, close-range photogrammetry is a well-known technique for 3D scanning of meso and large scale objects, while its application to small objects is still under experimentation. In the last few years, it has achieved a considerable development and it has been applied for industrial applications mainly because it allows a low cost, fast, and non-invasive scanning method. For example, in [3] it has been used for quality inspection of welds and for the measurement of the geometrical features of the detected defects, including

✉ Gianluca Percoco
gianluca.percoco@poliba.it

1 Dipartimento di Meccanica, Matematica e Management, Politecnico di Bari, Viale Japigia 182, 70126 Bari, Italy

2 Departamento de Ingeniería de Sistemas y Automática, Universitat Politécnica de Valencia, Camino de Vera 5, 46022 Valencia, Spain

surface flaws and imperfections, using a DSLR camera with a 50-mm lens mounted. In [4], another industrial application of photogrammetric methodology has been carried out. In particular, geometrical properties of a workpiece has been 3D digitized with the aim of obtaining a form of compensation to be involved in the computation of machining process parameters for the realization of revolution surfaces and threads. In [5], it has been implied as measurement methodology for sub-millimetric features.

Other applications can also be found in not strictly industrial research fields, such as [6] where close-range photogrammetry with macro lenses has been used for the characterization of cut marks on bones.

However, several aspects limit the applicability of this technology, particularly in the case of sub-millimeter features, due to the effect of some factors. There are several issues to be addressed: (a) when high magnifications are required, the angle of view (AOV) becomes smaller and the DOF gets narrower. Consequently, blurring becomes high and can influence considerably on the possibility of calibrating cameras accurately, (b) accuracy of pattern realization—the higher the magnification, the smaller and more accurate the pattern must be, and (c) the pinhole camera model is effective under several assumptions that cannot be verified for millimeter and micro-scale applications.

The use of non-metric cameras, indeed, requires the estimation of unknown parameters using specific mathematical models. In [7], 10 parameters such as focal length, principal point coordinates, and distortion parameters allow to reconstruct the internal camera geometry.

In [8], three kinds of correlation existing in the classical model, has been analyzed. The magnitude of correlation depends on a number of variables such as focal length. In general, the most significant correlation is that between the principal point and the tangential distortion leading to an error compensation in the parameters estimate.

Most 3D modeling commercial softwares [9] use SFM (structure from motion) algorithm to orient photographic images. This is because it allows a quick and automatic estimate of the intrinsic and extrinsic parameters within a scale factor.

In this context, quality assessment of intrinsic parameters is certainly a critical issue. In the computer vision literature, the most widely used parameter for this purpose is the reprojection error (RE). The algorithm analyzes photos, creates a virtual model where places points, analyzes again photos and compares the real points positions with the virtual ones, recalculates the position that every point should have, and finally computes the difference in terms of distance (expressed in pixels) between the corresponding two model points after a standard deviation analysis. The RE is computed for each photo and the result is a mean value. The lower the value, expectedly below one pixel, the more accurate is the model. For all these reasons, this issue is critical. From authors' knowledge, it is not possible to evaluate a priori, the quality, and accuracy of the calibration intrinsic parameters for a subsequent 3D reconstruction.

The purpose of this work is to study the performance of the photogrammetric technique, working with the classical pinhole camera model [7], and to digitize workpieces with micro-features of several geometrical complexities. In particular, with the aim of investigating the behavior of internal calibration and its influence on photogrammetric dimensional accuracy, 3D models have been retrieved using five different internal calibration sets, all of them characterized by sub-pixel values of RE [10].

In "Section 2", an overview of the actual state of the art in micro-photogrammetry is reported, in "Section 3", the calibration and 3D reconstruction procedure is described, while in "Section 4" the results are shown, both for calibration (4.1) and 3D measurement (4.2), and subsequently discussed (4.3).

2 Research background

Few solutions for the reconstruction of very small objects can be found in the photogrammetric literature and all of them are referable to the use of zoom lenses or macro lenses. In [11] a performance analysis of macro and zoom lenses has been conducted and it has been proved that the first ones are more preferable than the second ones because of lower distortion values and a greater stability in the calibration phase.

In fact, the adoption of macro lenses is subject to some disadvantages, such as the long distance between object and camera and the decrease of the angle of view (AOV) value.

In some research, the use of macro lenses in association with extension tubes has been proved to be a good solution [12–14]. The reasons are manifold, at first this combination is cheaper than macro lenses at high level of magnifications, and secondly it allows to work with shorter working distances, minimizing the loss of image quality if it is compared with other technologies.

There are, however, some disadvantages linked to this configuration, such as the loss of depth of field, which means that only a small region of the image is in focus.

In [5] and [15], a way to overcome the loss of focus has been implemented using multistack technology. The result is a good and cheap solution, easy to use and with accurate, acceptable results, but it performs well only with low magnifications.

The calibration of macro lenses has been a good topic in literature [11, 14, 16]. In [14], the calibration of a macro lens with two extension tubes, with magnification equal to 1.48× and 1.77×, has been obtained using classical calibration model and calibration patterns with only circular dots. The circular shape allows simplification of recognition phase.

In the newest computer vision photogrammetric software, the internal calibration can be computed automatically, together with the estimation of external recognition scene. In [12, 13], photogrammetry has been tested for the reconstruction of an artifact with sub-millimeter features and a high b/h ratio using the calibration model implemented in the Agisoft Photoscan software [9] for the alignment with good results but for low magnification levels.

3 Materials and methods

The experimental phase consisted of two steps:

1. Internal calibration.
2. 3D reconstruction.

3.1 Internal calibration

When calibration is performed, the pattern must be well known. This happens if the calibration pattern is accurately manufactured. The coordinates of the generic 3D point (p_x, p_y, p_z), center of the generic dot of the calibration pattern, together with its correspondences in the image (q_x, q_y), are used to compute the elements of the projection matrix. Considering λ as a scale factor, the generic 3D point will correspond to the i^{th} 2D point on the image according to the following:

$$q = \lambda M p \quad \forall \lambda \in \mathfrak{R} \tag{1}$$

$$\begin{bmatrix} q_x \\ q_y \\ 1 \end{bmatrix} = \lambda \begin{bmatrix} m_{11} & m_{12} & m_{13} & m_{14} \\ m_{21} & m_{22} & m_{23} & m_{24} \\ m_{31} & m_{32} & m_{33} & m_{34} \end{bmatrix} \begin{bmatrix} p_x \\ p_y \\ p_z \\ 1 \end{bmatrix} \tag{2}$$

Camera calibration is a mature procedure in close-range photogrammetry, but it is not clear if the camera models used in close range are valid for micro-features detection. Therefore, calibration issue continues to receive research attention to define the limits of the standard models. The state-of-the-art in photogrammetric camera calibration has been considered by several publications, e.g., [17] and [18]. The task of camera calibration has also been addressed by the computer vision community. Computer vision researchers have developed fully automated calibration procedures. These procedures started using 3D patterns [19], but later the calibration procedures were simplified using 2D and 1D patterns [20, 21]. Several camera calibration techniques exist, but the present paper dwells on the calibration method based on a bi-dimensional pattern, since the camera is calibrated using several images of a planar pattern easily.

Normally, real lenses that induce distortions in the camera model must be considered and corrected before the computation of M. Most camera modeling approaches are based on additional parameters for modeling deviations between the ideal mathematical model of central perspective and the physical reality of the camera. Several distortion models are known in the literature [22] (e.g., field-of-view distortion model, division model, or rational function distortion model) but, in the present application, the classic radial and tangential distortion model is considered valid to correct the low distortions produced by the vision system.

$$\overline{x} = q'_x - c_x \tag{3}$$

$$\overline{y} = q'_y - c_y \tag{4}$$

$$\Delta x = \overline{x}r^2 k_1 + \overline{x}r^4 k_2 + \overline{x}r^6 k_3 + \left(2\overline{x}^2 + r^2\right)p_1 + 2p_2\overline{x}\,\overline{y} \tag{5}$$

$$\begin{aligned} \Delta x &= \overline{x}r^2 k_1 + \overline{x}r^4 k_2 + \overline{x}r^6 k_3 + \Delta y \\ &= \overline{y}r^2 k_1 + \overline{y}r^2 k_1 + \overline{y}r^4 k_2 + \overline{y}r^4 k_2 + \overline{y}r^6 k_3 \\ &\quad + \left(2\overline{y}^2 + r^2\right)p_2 + 2p_1\overline{x}\,\overline{y} \end{aligned} \tag{6}$$

$$q_x = \overline{x} + \Delta x \tag{7}$$

$$q_y = \overline{y} + \Delta y \tag{8}$$

where (q'_x, q'_y) are the distorted image coordinates, (c_x,c_y) are the principal point coordinates, (Δx, Δy) are the distortion corrections of the image coordinates, (k_1, k_2, k_3) are the radial distortion factors, (p_1, p_2) are the tangential distortion factors, and finally (q_x, q_y) are corrected image coordinates.

Second, the intrinsic (α_x,α_y,c_x,c_y) and extrinsic parameters (R, t) are extracted from the projection matrix M defined in Eqs. (1) and (2):

$$\begin{bmatrix} m_{11} & m_{12} & m_{13} & m_{14} \\ m_{21} & m_{22} & m_{23} & m_{24} \\ m_{31} & m_{32} & m_{33} & m_{34} \end{bmatrix} = \lambda \begin{bmatrix} \alpha_x & s & c_x \\ 0 & \alpha_y & c_y \\ 0 & 0 & 1 \end{bmatrix} [\mathbf{R}\ \mathbf{t}] \tag{9}$$

The intrinsic parameters are the focal lengths in pixels (α_x,α_y), the principal point coordinates in the image coordinate system (c_x,c_y) and the skew factor s which is conventionally considered zero in computer vision, while λ is the same scale factor as in Eqs. (1) and (2). The extrinsic parameters define the location of the scene reference system with respect to the camera reference system, being R a 3 × 3 rotation matrix and t a 3 × 1 offset vector. In photogrammetry, the internal calibration is important since it consists of finding the intrinsic parameters and the distortion parameters of correction, namely: k_1, k_2, k_3, p_1, and p_2.

In this context, the RE of an image point is the geometric error corresponding to the image distance between a theoretical projected point (q_i) and a measured one ($\widehat{q_i}$). It is used to quantify how closely a theoretical projection (q_i) of a 3D point

(Q_i) recreates the point's measured projection ($\widehat{q}_i$). Precisely, let M be the projection matrix of a camera and q_i be the measured image projection of Q_i, i.e., $\widehat{q_i} = MQ_i$. The RE of Q_i is given by $d(q_i, \widehat{q}_i)$, where $d(q_i, \widehat{q}_i)$ denotes the Euclidean distance between the image points represented by vectors q_i and $\widehat{q}_i$.

RE [20] is defined as the geometric error corresponding to the average image distance, measured in pixels, between a point, projected according to the camera calibration model, and its corresponding measured counterpart. RE of a set of points is calculated as follows:

$$\mathrm{RE} = \frac{\sum_i d\left(qi, \widehat{q}i\right)}{n} \tag{10}$$

where n is the number of points.

In this work, the open source software library Open CV has been used and it offers three types of calibration patterns: symmetric, asymmetric, and checkboard. Preliminary studies [23] established that patterns with circular dots are less sensitive to blurring than calibration checkerboard, allowing the recognition of the dots when they are not in focus. In this case, a symmetric calibration pattern has been used. It consists of 22 columns and 18 rows of photoetched dots (chrome on glass) as shown in Fig. 1.

Each dot has a diameter of 0.25 mm and the distance between two adjacent ones is equal to 0.5 mm.

Five sets of photographs were acquired for each configuration of macro lens and extension tubes, and processed using the functions of the OpenCV library [24], version 2.4.11, for the estimation of the intrinsic parameters.

The experiment was conducted using a digital reflex camera Canon Eos 400D with a 10 megapixel resolution (3888 × 2592 pixel^2) and a APS-C CMOS sensor (22.2 × 14.8 mm^2). A Canon EF-S 60 mm F2.8 macro lens, with the focus distance set to its minimum value, was used adding extension tubes to obtain 44, 52, and 60 mm of total extension. The configurations obtained correspond to lateral resolutions of 2.9, 2.7, 2.4 μm, and vertical resolutions of 5.8, 5.4, 4.8 μm, and magnification levels of 2.06×, 2.23×, and 2.4×.

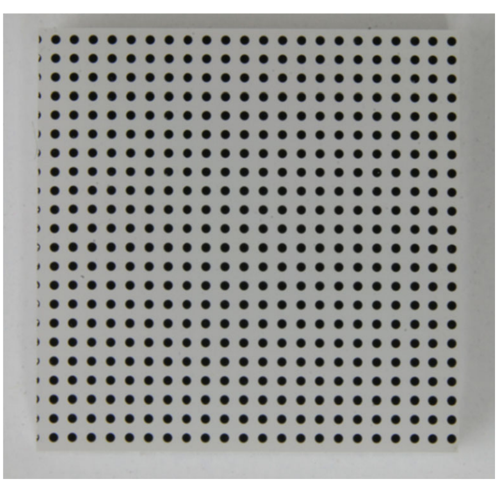

Fig. 1 Symmetric calibration pattern

Each calibration set consists of 24 images is obtained by tilting the pattern gradually along the three axis, taking care to keep the center in focus, according to [25].

OpenCV calibration tool runs an automatic dot recognition procedure. The recognition of dots is based on the well-known OpenCV BLOB- (binary large object) detection method. This consists of calculating the centroids of the connected blob, with sub-pixel precision. In addition, blob detection method allows filtration of returned blobs by color, area, circularity, etc. Default values of these filter parameters are tuned to extract dark circular blobs. In general, OpenCV calibration can be run without any adjustment of these default parameters, but in our specific research, the default values had to be adjusted to detect dots. The authors observed that the OpenCV 3.1 calibration routines did not manage images with lateral dimensions higher than 1 Mpixel [25]. In fact, the OpenCV function *findCirclesGrid* attempts to determine whether the input image contains a grid of circles, it locates the centers of the circles, returning a non-zero value, if all the centers have been found and placed in the correct order (row by row, left to right in every row). If the function fails, it returns 0. The OpenCV source code was corrected by the authors in order to deal with higher resolution images.

3.2 3D measurement

The quality of the calibration parameters was tested by 3D reconstruction of two workpieces (Fig. 2), showing a prismatic shape with a sub-millimeter etching (workpiece 1) and a concave gear wheel shape (workpiece 2).

Both workpieces have been chosen to test the system under different conditions. Workpiece 1 was selected because of its sharp edges, geometrically regular features and a micro-etching on the top, while the concave geometry and small details were the reasons for choosing workpiece 2. The manufacturing technology chosen was electro discharge machining for its capability to generate textured surfaces very appropriate for photogrammetry.

Figures 3,4,5 consist of a white box illuminated from all sides with a led strip integrated to the workpiece located at the center of the box, positioned at the center of a turning table ISEL-RFII, with an angular position resolution equal to 3°. During the surveys, according to [26], the rotation angle of the table was set at 5° and the camera was tilted with respect to the table at 45°. This choice derives from previous experiences [12], and it is the best tradeoff for both artifacts which are geometrically different. A high-tilt angle value, up to 60°, is preferable for objects with high depth values such as deep holes, while for objects with lower deep values also lower- tilt angles work well. For both workpieces, three acquisition sets were realized, one for each configuration lens-extension tube.

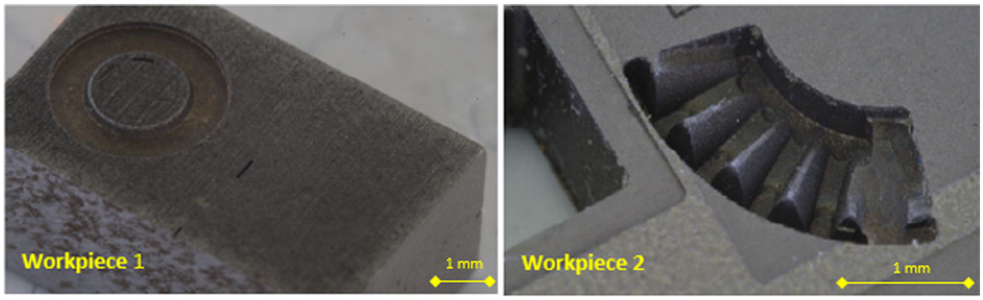

Fig. 2 Test workpieces: *prismatic shape* on the left (workpiece 1) and *concave gear wheel shape* (workpiece 2)

The resulting 72 images for each workpiece and for each extension tube configuration were processed by AgisoftPhotoscan, software version 1.1.6, using the fixed internal calibration, pre-computed with the aid of the OpenCV library software.

The phases in which the reconstruction process are articulated are basically two: the alignment phase and the dense surface modeling phase.

The alignment includes two sub-steps: detection of key points on the images, and processing of these data to estimate external and internal calibration parameters simultaneously. In this case, the feature detection is made by a similar descriptor to scale invariant feature transform (SIFT) descriptor [27], while the computation of the internal and external calibration parameters is carried out by a Structure-from-Motion algorithm (SFM).

SIFT is an object recognition method that allows image-recognizing features suitable for matching different images in a scene. The features must be invariant to image scaling and rotation, and partially invariant to change in illumination and 3D camera view point. The output of the process is a large collection of feature vectors called SIFT keys, which describe the local image region sampled. These vectors are the input for the next phase, the first and approximate intrinsic and extrinsic parameters estimate. Subsequently, the bundle adjustment method [28] is exploited, which is substantially an optimization method leading to the computation of some unknown parameters by the minimization of cost function. In the photogrammetric case, the cost function to minimize is the RE of the photogrammetric elaboration.

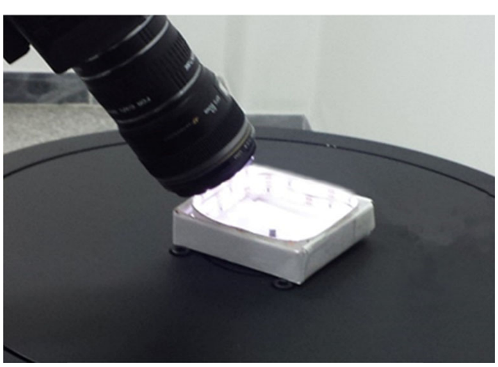

Fig. 3 Experimental set

4 Results

4.1 Calibration

In the experimentation, five calibration certificates were realized for each configuration lens-extension tube to evaluate the repeatability of the methodology adopted.

The first configuration involves the use of a 44-mm extension, obtained as the sum of a 20-mm extension tube and two 12-mm extension tubes. The camera models obtained in this configuration are reported in Table 1.

The second and the third configuration, reported below in Table 2 and Table 3, are characterized by 52 and 60 mm, respectively, with 32 mm plus 20 mm and 36 mm plus two 12-mm extension tubes.

The analyses of the three tables put in evidence the stability of the focal length parameters in all the conditions computed as the average between α_x and α_y, assuming that the sensor of the camera used is composed of square pixels. The standard deviation of the focal length parameters computed over the five iterations resulted in less than 0.2%, with a maximum value of 0.5% for the 60-mm configuration. Conversely, the position of the principal point identified by C*x* and C*y* coordinates, highlights huge variations since its correlation with the tangential distortion parameters is widely known p_1 and p_2 [8].

This type of correlation is essentially caused by the polynomial representation of the calibration model, consisting of a resolution of a hyper linked equation system leading to a high sensitivity of the principal point coordinates values, as the tangential distortion values change and vice versa.

Moreover, it can be appreciated that when principal points in two different rows are similar, then the estimated radial and tangential distortions parameters are also similar.

4.2 3D measurement

All necessary tests were carried out using the images as input of the commercial software Agisoft Photoscan version 1.1.6, changing the calibration intrinsic parameters as resulting from the predetermined calibrations.

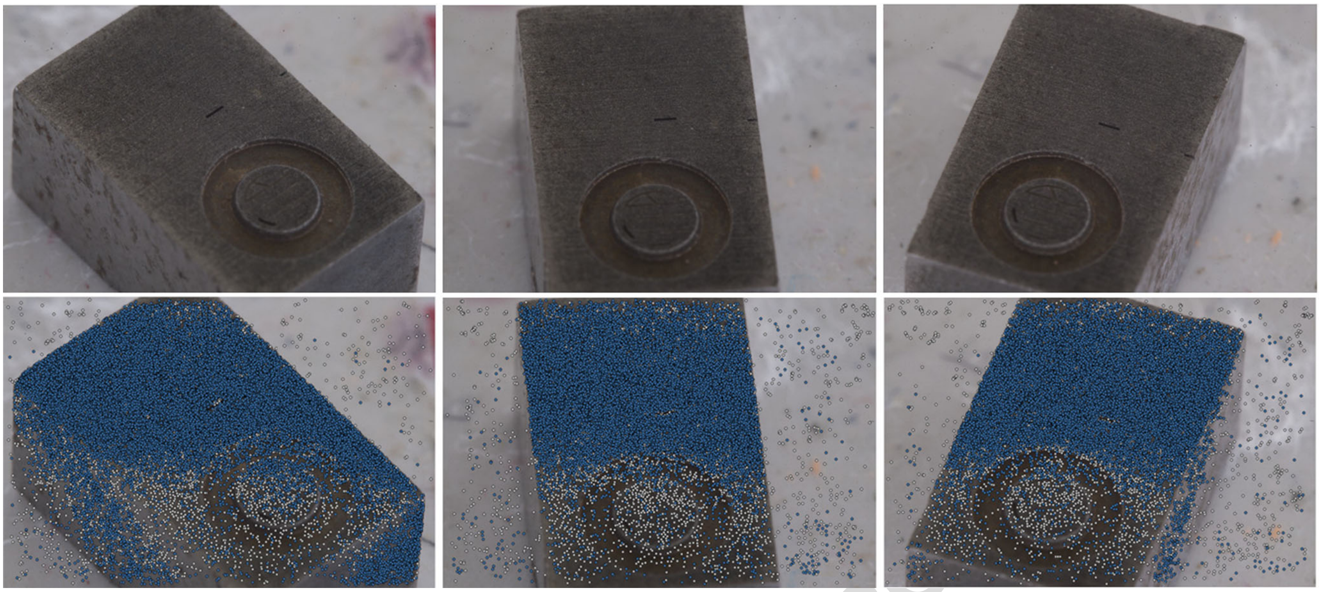

Fig. 4 Above, example of three pictures taken from different positions and below, tie points recognized on them

For each workpiece, one mesh for each calibration set was retrieved and compared to that obtained using the optical profilometer Taylor Hobson CCI MP-HS, equipped 10× with a displacement resolution of 0.01 nm on z-axis and a scan range up to 2.2 mm without stitching. The comparison was accomplished after an iterative closest point (ICP) procedure, with the commercial software geomagic control. Each photogrammetric mesh was computed with measured and predetermined data camera calibration, and the profilometer mesh obtained from the point cloud comprising more than 13 million points.

The reconstruction of both workpieces has been realized with the same camera configuration used in the calibration phase, achieving a textured mesh of the object for each calibration certificate.

After elaboration, there is still a parameter unsolved: the scale factor λ shown in Eqs. (1), (2), and (9). During the photogrammetric alignment, this value is assumed as a random parameter whose value can change at each processing, with the same input data and conditions. This is a very important issue related to the photogrammetric technique. The possible scaling methods are essentially the following: (i) using a known distance between two markers within the images; (ii) placing the camera/s in known positions or at a known distance between each other. Method (i) has disadvantages for small measurement volumes: the higher the magnification, the lower the field of view, leading to very small markers with increasing costs and blurring. Method (ii) can be reproduced in micro-measurements, only with more complex procedures and instruments to obtain accurate external calibration.

Given the availability of very accurate point clouds of the workpieces, the scale has been obtained by exploiting one method programmed into the open source scientific software, MeshLab [29]. This software allows one to scale a model with respect to another one, choosing a number of homologous points to match.

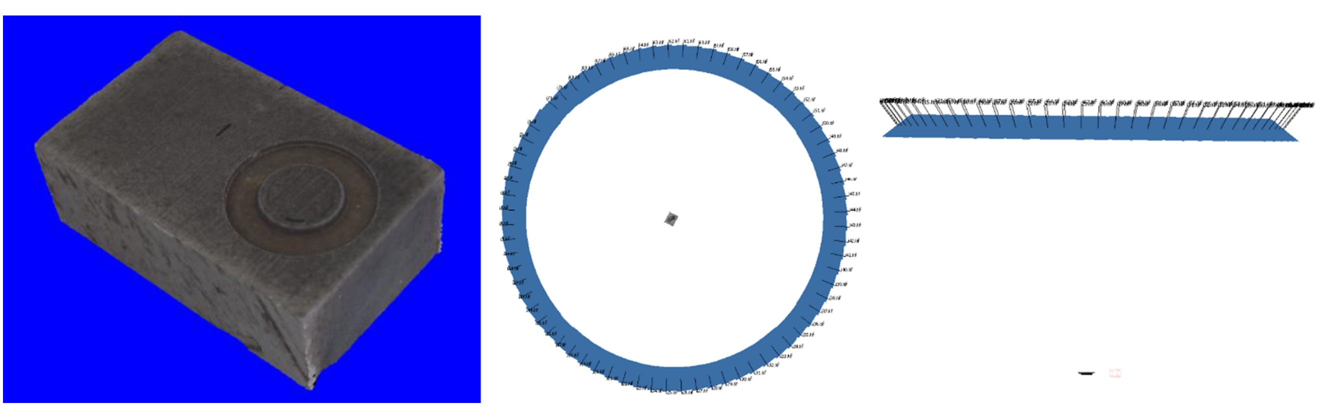

Q3 **Fig. 5** Final 3D reconstruction of the object and the entire shooting scenario (camera positions are represented by a *circle*)

Table 1 Calibration results with 44-mm extension tube

Camera models with 44-mm configuration (lateral resolution 2.9 μm, vertical resolution 5.8 μm)

Set	RE (p_x)	α_x (p_x)	α_y (p_x)	c_x (p_x)	c_y (p_x)	k_1	k_2	k_3	p_1	p_2
1	0.4263	65,870.69	65,880.77	2065.16	1307.12	1.5946	360.74	0.4980	0.0007	0.0047
2	0.4155	65,564.57	65,608.18	1961.60	1989.38	2.0077	−173.12	−0.3598	−0.0021	−0.0051
3	0.6427	65,851.69	65,839.04	1298.78	1369.82	1.5778	185.36	0.2567	0.0022	−0.0210
4	0.4838	65,778.12	65,804.27	1895.61	1837.24	2.2844	−305.83	−0.5914	0.0189	−0.0009
5	0.3214	65,686.86	65,712.28	1938.61	1811.21	2.1117	−228.71	−0.3943	0.0185	0.0005

Table 2 Calibration results with 52-mm extension tube

Camera models with 52-mm configuration (lateral resolution 2.7 μmvertical resolution 5.4 μm)

Set	RE (p_x)	α_x (p_x)	α_y(p_x)	c_x (p_x)	c_y (p_x)	k_1	k_2	k_3	p_1	p_2
1	0.4947	70,223.93	70,238.77	1375.52	1718.93	1.78799	188,364	0.21735	0.01431	−0.01696
2	0.2184	70,599.25	70,631.25	1791.18	1238.46	1.42737	603,097	0.78745	−0.00207	−0.00507
3	0.1739	70,367.70	70,402.56	1877.66	1281.65	1.51894	474,452	0.607	0.00018	−0.00221
4	0.494	70,391.10	70,386.92	2311.47	1297.78	1.96254	−32,248	−0.07302	−0.00236	−0.01381
5	0.5621	70,381.50	70,380.16	2365.07	1308.94	1.97972	−121,935	−0.18118	0.00302	0.01480

At each iteration of the well-known iteration closest point (ICP) algorithm, the software computes the transformation matrix for roto-translation and the scale factor for the photogrammetric mesh to match the one under reference, thereby minimizing the Euclidean distance between homologous points.

If more points are chosen and lower is the original difference in scale between the two models, the scaling process will be more accurate. In this work, the reference model was obtained with an interferometric profilometer Taylor Hobson CCI MP-HS, and a magnification level of 10× which means an optical resolution of 1.3 μm. A stitching scan was necessary because the size along *x*- and *y*-axis exceeded the field of view of the single scan (Fig. 6 and Fig. 7).

Subsequently, each scaled model has been compared with the reference one.

4.3 Discussion of results

Data obtained from the 3D comparisons are reported in Fig. 8 and have been retrieved exploiting the commercial software geomagic control after a new best-fit alignment between the interferometric scan data, identified as the reference and photogrammetric scan data, identified as the system under test. After the manual identification of three points, the ICP algorithm [30] finds the nearest point of the test for each point of the reference and computes the Euclidean distance. Each point of the test is associated with a distance and the distances are clustered into colored intervals, according to the legend reported on the top of Fig. 8.

Some regions are not involved in the comparison, such as vertical sides, with a slope value close to 90°, but this must be addressed to the limits of the interferometric technique.

Table 3 Calibration results with 60-mm extension tube

Camera models with 60-mm configuration (lateral resolution 2.4 μmvertical resolution 4.9 μm)

Set	RE (p_x)	α_x (p_x)	α_y (p_x)	c_x (p_x)	c_y (p_x)	k_1	k_2	k_3	p_1	p_2
1	0.34513	77,045.94	77,037.73	1614.08	1430.8	1.9501	120,694	0.15899	0.00428	−0.00795
2	0.73743	77,888.89	77,920.03	2138.93	1823.54	2.5302	−467,351	−0.63685	0.01633	0.00693
3	0.63748	77,804.52	77,854.23	2109.72	2060.41	2.8983	−744,123	0.02394	0.02394	0.00635
4	0.785	77,133,61	77,161.3	2243.69	1000.44	1.5703	464,916	0.66882	−0.0108	0.0107
5	0.72016	77,327.01	77,337.6	1934.02	1643.74	2.0557	−1,2035	−0.00216	0.00920	0.00080

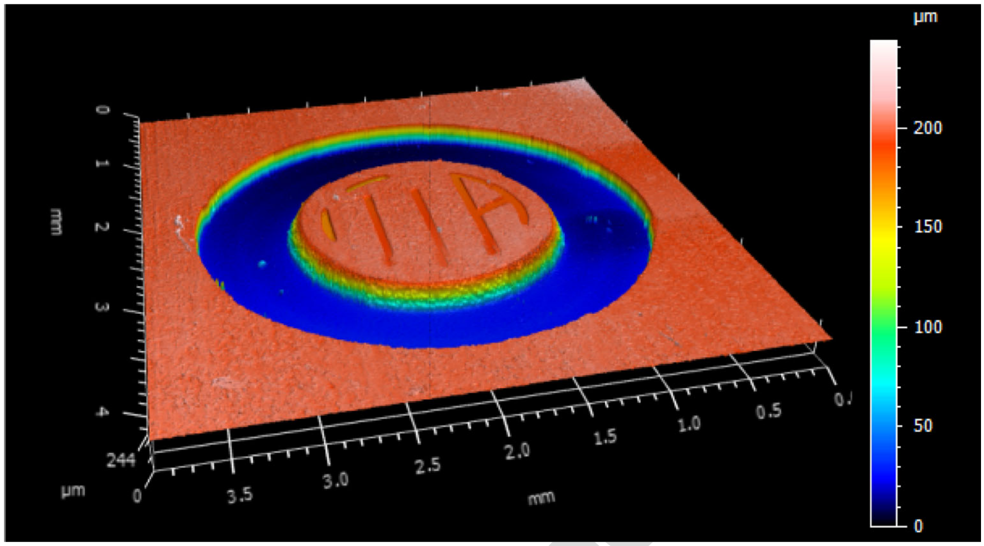

Fig. 6 Image of workpiece 1 reconstructed with Taylor Hobson CCI MP-HS

In general, comparisons involved a high number of points (about 350,000 for each comparison) with a low percentage of discarded points (2.8% is the higher case).

In the graph shown in Fig. 9, the average deviations between the reference model and the test models are reported for each magnification (extension tube), and each calibration set.

After the alignment, geomagic control returns the average positive and negative distances, between two homologous points and the standard deviation of distances.

In this case, two response parameters have been chosen: the average distance computed as the arithmetical average between the absolute values of average deviations (positive and negative), and the standard deviation of distances to be compared, with other parameters as the minimal resolutions achievable with the implemented system.

Moreover, a 3 σ statistical analysis has been carried out for each combination, on the average distance computed by 3D comparisons. The five average distances computed for each workpiece and extension tube have been taken into account for the analysis and their Gaussian distribution is shown in Fig. 10 (left side). In all the cases, the probability of obtaining a value of the average distance very close to the mean value is high. UCL (upper control limit) and LCL (lower control limit) are computed as mean value ±3 σ, and shown in Fig. 10 (right

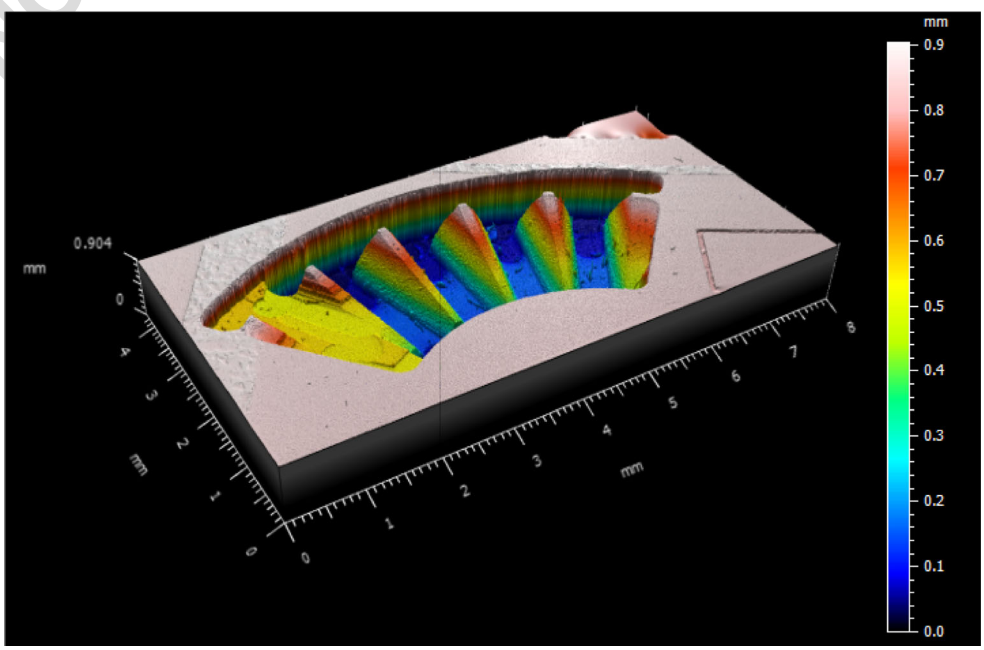

Fig. 7 Image of workpiece 2 reconstructed with Taylor Hobson CCI MP-HS

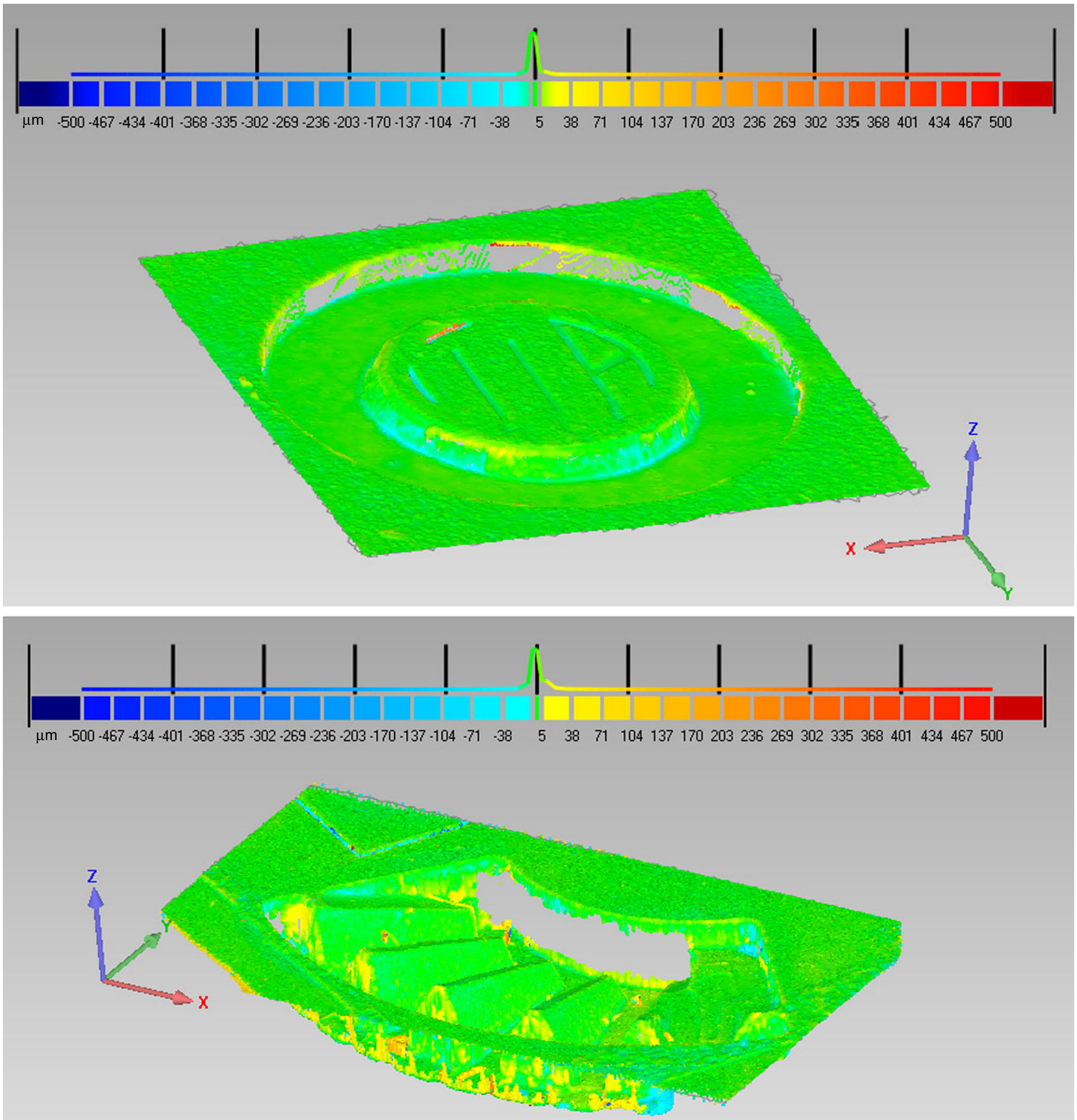

Fig. 8 3D comparison results between the best photogrammetric and reference models

side). The different calibrations do not have appreciable influence on the average distances computed.

In general, both reconstructions led to good results, with average deviations of few micrometers for workpiece 1 and 10 µm for workpiece 2. A direct influence of the calibration set was not evident, being the maximum variabilities for each workpiece, with each extension tube lower than 5 µm. It must be underlined that all the calibrations achieved a sub-pixel RE, leading to be considered as very accurate.

This difference is due to the different geometrical complexity of the benchmarks. For workpiece 1, the shape is very simple and the maximum depth is 244 µm; the workpiece 2, instead, can be classified as a very complex object because of its cave geometry (with maximum depth of 904 µm), which also makes the penetration of light difficult. Further considerations can be done by comparing the results obtained from average deviations with the resolutions of the system for each configuration implemented.

The resolution parameters change with the configuration, and magnification level used.

For workpiece 1, the average distances comprise lateral and vertical resolution value. The mostly flat geometry of the piece and the value of maximum depth very close to the DOF (depth of focus) value ensured by the system implemented (about 200 µm) allowed to obtain results very close to the limits of resolution. Different considerations can be done for the workpiece 2. In this case, the average distance values are always more than the lateral and vertical resolutions, up to three times the vertical resolution in the worst case registered. To explain these results, other factors have to be taken into

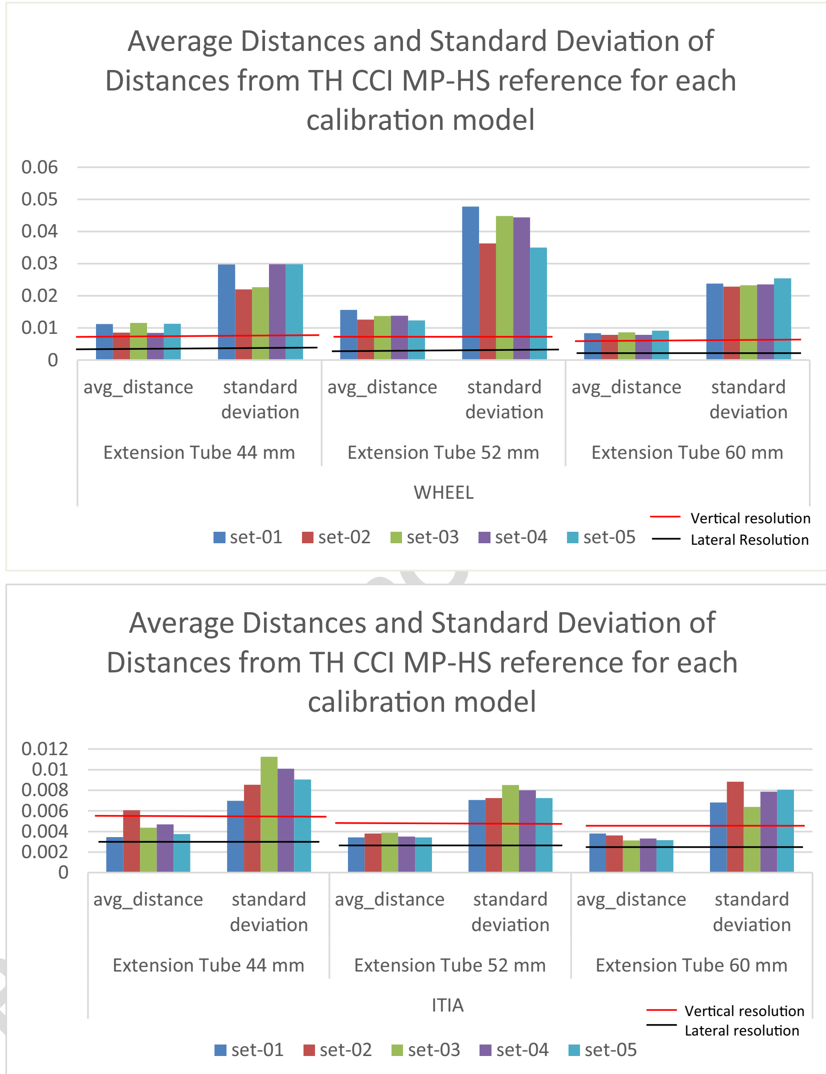

Fig. 9 Average deviations distribution with minimal resolution limits

account, such as the magnification level and the problems related to the penetration of light, especially in the area with the maximum depth value. The colored map, presented in Fig. 6, puts in evidence that the highest deviation values correspond, for workpiece 2, to the outlying areas with the highest values of depth. This aspect has more impact in the first two configurations, with slightly lower magnification level and minimal higher vertical resolution value, as well as a lower capability of light to achieve the deepest areas.

However, the best results have been obtained for both benchmarks, with the third configuration (60-mm extension tube), with average distances registered at 3 μm for workpiece 1 and an average distance slightly lower than 10 μm for workpiece 2. In particular, this difference is more prominent for the workpiece 2 (the average deviation changes from 8 to 15 μm), while for the workpiece 1 all three configurations led to good and very close results.

Further considerations can be done for the deviation registered on vertical sides of both objects mainly due to the limit of the interferometer instrument, whose maximum slope value, for the magnitude level selected is equal to 10.5°.

5 Conclusions

In this paper, the calibration parameters, computed with the traditional pinhole camera model have been tested for magnification levels higher than 2×.

With the aim of verifying if the camera model can be applied to magnifications higher than 2×, not yet in literature until now, experiments have been set up using a reflex camera with a 60-mm macro lens equipped with the combination of three extension tubes, corresponding to 2.06, 2.23, and 2.4 magnification levels, respectively.

Experimentation consisted of repeating calibration five times for each configuration and testing each calibration model, measuring two artifacts with different geometrical complexity. The calibration results have pointed good

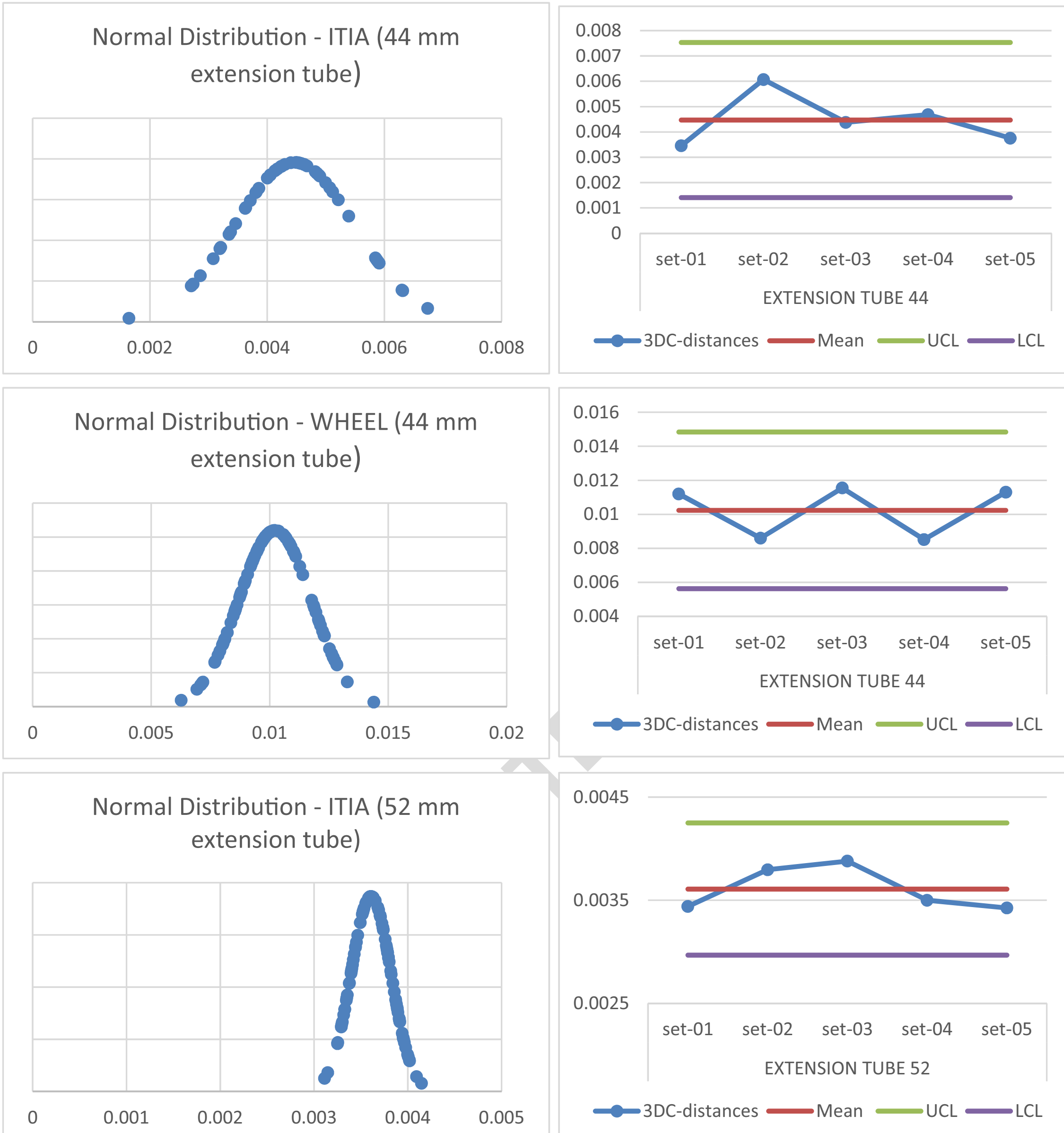

Fig. 10 3-sigma statistical control of average distances computed in 3D comparisons and Gaussian distribution fitted for each data set

repeatability in the computation of the focal length parameters (st. dev. less than 0.5% in the worst case), and a higher variability of the principal point coordinates justified by the known high correlation between this value and the tangential distortion values. After the 3D model retrieval and the scaling process of the model, the comparisons with the reference model, identified by the absolute average and standard deviation of the Euclidean distances computed between each point of the test model and the corresponding point on the reference, led to two considerations.

Initially, they confirm the repeatability of the internal calibration parameters. Despite the differences from OpenCV for each calibration, a lower reprojection error obtained in the calibration process does not guarantee a better result of the photogrammetry method.

Second, they highlight the performance of the photogrammetric system presented, equipped for very high magnification level, to realize 3D reconstruction with an uncertainty of few micrometers comparable with the industry's best technologies and to reconstruct cave and complex objects with a good level of accuracy.

Other experiments will be conducted to improve the photogrammetric scanning methodology of very deep areas using more than one tilt angle position of camera.

Furthermore, since the behavior of photogrammetry is strongly affected by the scaling method, further studies must be conducted on this aspect to achieve a robust scaling method for micro-photogrammetry.

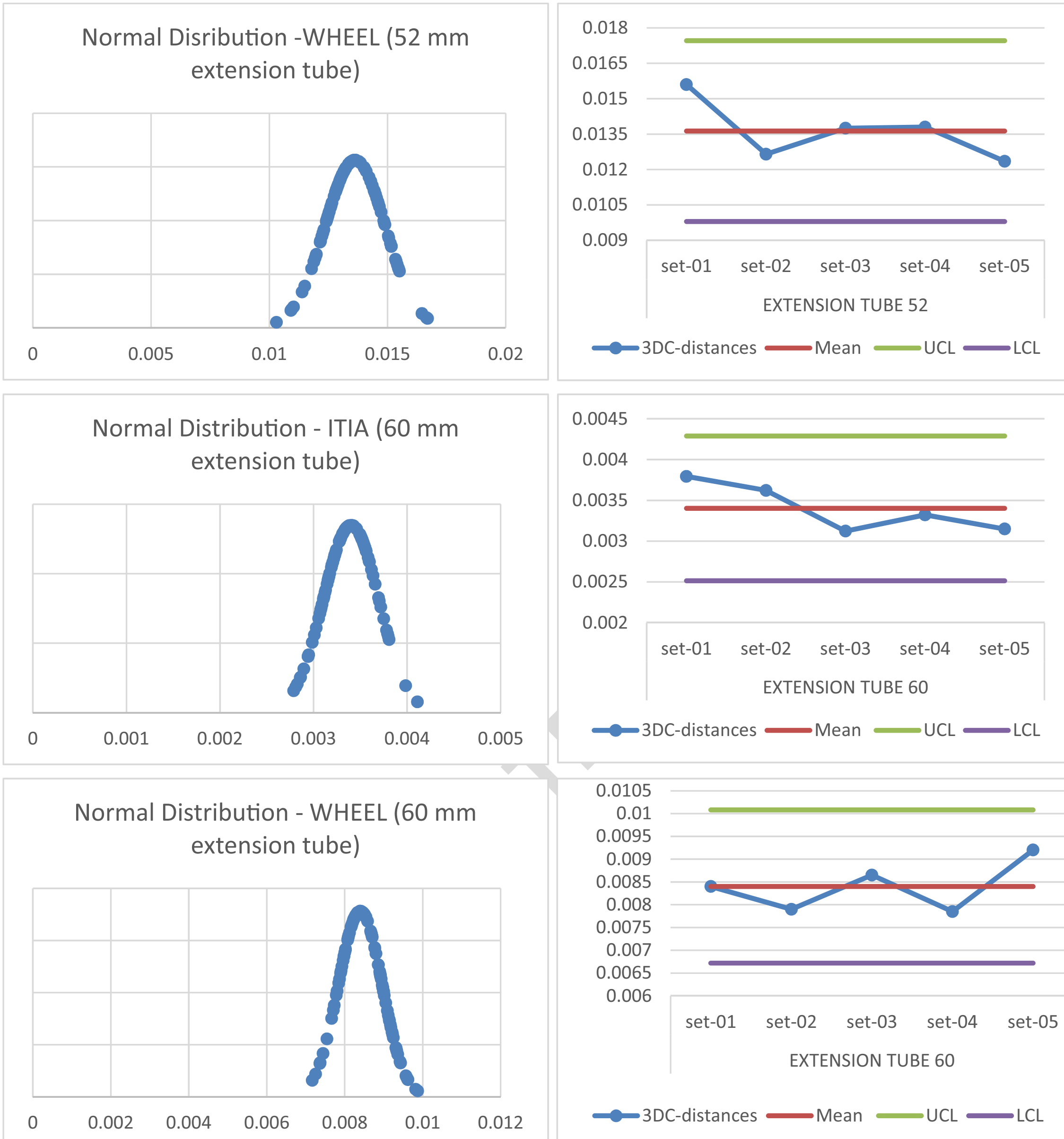

Fig. 10 continued.

Acknowledgement The workpieces were kindly shared by Dr. Francesco Modica and Dr. Gianluca Trotta from the Institute for Industrial Technologies and Automation of the Italian National Research Council.

References

1. Uhlmann E, Mullany B, Biermann D, Rajurkar KP, Hausotte T, Brinksmeier E (2016) Process chains for high-precision components with micro-scale features. CIRP Ann - Manuf Technol 65: 549–572. doi:10.1016/j.cirp.2016.05.001
2. Savio E, De Chiffre L, Schmitt R (2007) Metrology of freeform shaped parts. CIRP Ann - Manuf Technol 56:810–835. doi:10.1016/j.cirp.2007.10.008
3. Rodríguez-martín M, Lagüela S, González-aguilera D, Rodríguez-gonzálvez P (2015) Optics & Laser Technology Procedure for quality inspection of welds based on macro-photogrammetric three-dimensional reconstruction;73:54–62
4. Xu Z, Toncich D, Stefani S (1999) Vision-based measurement of three-dimensional geometric workpiece properties. Int J Adv Manuf Technol 15:322–331. doi:10.1007/s001700050074
5. Galantucci LM, Lavecchia F, Percoco G (2013) Multistack close range photogrammetry for low cost submillimeter metrology. J Comput Inf Sci Eng 13:44501. doi:10.1115/1.4024973
6. Domínguez-rodrigo M, Palomeque-gonz JF (2015) Micro-photogrammetric characterization of cut marks on bones. Gonz a b 62.
7. Brown DC (1971) Close-range camera calibration. Photogramm Eng 37:855–866 doi:10.1.1.14.6358
8. Tang R, Fritsch D (2013) Correlation analysis of camera self-calibration in close range photogrammetry. Photogramm Rec 28: 86–95. doi:10.1111/phor.12009

9. Agisoft LLC (2011) Agisoft PhotoScan User Manual :37.
10. Jcgm JCFGIM (2008) Evaluation of measurement data—guide to the expression of uncertainty in measurement- annex B "general metrological terms"- B.2.14. Int Organ Stand Geneva ISBN 50: 134. doi:10.1373/clinchem.2003.030528
11. Information S, Division T (n.d.) Performance evaluations of macro lenses. Archives 1–6
12. Galantucci LM, Pesce M, Lavecchia F (2015) A stereo photogrammetry scanning methodology, for precise and accurate 3D digitization of small parts with sub-millimeter sized features. CIRP Ann - Manuf Technol 64:507–510. doi:10.1016/j.cirp.2015.04.016
13. Galantucci LM, Pesce M, Lavecchia F (2015) A powerful scanning methodology for 3D measurements of small parts with complex surfaces and sub millimeter-sized features, based on close range photogrammetry. Precis Eng. doi:10.1016/j.precisioneng.2015.07.010
14. Percoco G, Antonio JS (2015) Photogrammetric measurement of 3D freeform millimetre-sized objects with micro features: an experimental validation of the close-range camera calibration model for narrow angles of view;0
15. Gallo A, Muzzupappa M, Bruno F (2014) 3D reconstruction of small sized objects from a sequence of multi-focused images. J Cult Herit 15:173–182. doi:10.1016/j.culher.2013.04.009
16. Stamatopoulos C, Fraser CS, Cronk S (2010) On the self-calibration of long focal length lenses. Int Arch Photogramm Remote Sens Spat Inf Sci Newcastle upon Tyne, UK 2010 XXXVIII:560–564
17. Atkinson KB (1996) Close range photogrammetry and machine vision. Whittles Publishing
18. Luhmann T, Fraser C, Maas HG (2016) Sensor modelling and camera calibration for close-range photogrammetry. ISPRS J Photogramm Remote Sens 115:37–46. doi:10.1016/j.isprsjprs.2015.10.006
19. Tsai RY (1986) An efficient and accurate camera calibration technique for 3D machine vision. Proc IEEE Conf Comput Vis Pattern Recognition 1986
20. Ricolfe-Viala C, Sanchez-Salmeron A-J (2011) Camera calibration under optimal conditions. Opt Express 19:10769–10775. doi:10.1364/OE.19.010769
21. Wang L, Wang W, Shen C, Duan F (2016) A convex relaxation optimization algorithm for multi-camera calibration with 1D objects. Neurocomputing
22. Ricolfe-Viala C, Sanchez-Salmeron *A. Lens* distortion models evaluation. Appl Opt 2010;49:5914–5928.
23. Percoco G, Lavecchia F, Salmerón AJS (2015) Preliminary study on the 3D digitization of millimeter scale products by means of photogrammetry. Procedia CIRP 33:257–262. doi:10.1016/j.procir.2015.06.046
24. Bradski G (2000) The OpenCV Library. Dr Dobb's J Softw Tools
25. Percoco G, Sánchez Salmerón AJ (2015) Photogrammetric measurement of 3D freeform millimetre-sized objects with micro features: an experimental validation of the close-range camera calibration model for narrow angles of view. Meas Sci Technol 26:95203. doi:10.1088/0957-0233/26/9/095203
26. Ricolfe-Viala C, Sanchez-Salmeron A-J (2011) Optimal conditions for camera calibration using a planar template. 2011 18th IEEE. Int Conf Image Process, IEEE 2011:853–856. doi:10.1109/ICIP.2011.6116691 Q5
27. Lowe DG (1999) Object recognition from local scale-invariant features. Proc Seventh IEEE Int Conf Comput Vis 2:1150–1157. doi:10.1109/ICCV.1999.790410
28. Triggs B, Mclauchlan P, Hartley R, Fitzgibbon A, Triggs B, Mclauchlan P, et al. (2010) Bundle adjustment—a modern synthesis to cite this version: bundle adjustment—a modern synthesis
29. Cignoni P, Callieri M, Corsini M, Dellepiane M, Ganovelli F, Ranzuglia G (2008) Meshlab: an open-source mesh processing tool. Eurographics Ital Chapter Conf 2008:129–136
30. Besl P, McKay N (1992) A method for registration of 3-D shapes. IEEE Trans Pattern Anal Mach Intell 14:239–256. doi:10.1109/34.121791